AIP Journal of Applied Physics

Mechanical behavior of a composite interface: Calcium-silicate-hydrates

Steven D. Palkovic, Sina Moeini, Sidney Yip, and Oral Büyüköztürk

Citation: Journal of Applied Physics **118**, 034305 (2015); doi: 10.1063/1.4926870
View online: http://dx.doi.org/10.1063/1.4926870
View Table of Contents: http://scitation.aip.org/content/aip/journal/jap/118/3?ver=pdfcov
Published by the AIP Publishing

Mechanical behavior of a composite interface: Calcium-silicate-hydrates

Steven D. Palkovic,[1] Sina Moeini,[1] Sidney Yip,[2] and Oral Büyüköztürk[1,a)]
[1]Department of Civil and Environmental Engineering, Massachusetts Institute of Technology, Cambridge, Massachusetts 02139, USA
[2]Department of Nuclear Engineering, Massachusetts Institute of Technology, Cambridge, Massachusetts 02139, USA

(Received 1 May 2015; accepted 5 July 2015; published online 17 July 2015)

The generalized stacking fault (GSF) is a conceptual procedure historically used to assess shear behavior of defect-free crystalline structures through molecular dynamics or density functional theory simulations. We apply the GSF technique to the spatially and chemically complex quasi-layered structure of calcium-silicate-hydrates (C-S-H), the fundamental nanoscale binder within cementitious materials. A failure plane is enforced to calculate the shear traction-displacement response along a composite interface containing highly confined water molecules, hydroxyl groups, and calcium ions. GSF simulations are compared with affine (homogeneous) shear simulations, which allow strain to localize naturally in response to the local atomic environment. Comparison of strength and deformation behavior for the two loading methods shows the composite interface controls bulk shear deformation. Both models indicate the maximum shear strength of C-S-H exhibits a normal-stress dependency typical of cohesive-frictional materials. These findings suggest the applicability of GSF techniques to inhomogeneous structures and bonding environments, including other layered systems such as biological materials containing organic and inorganic interfaces. [http://dx.doi.org/10.1063/1.4926870]

I. INTRODUCTION

The deformation and strength behavior of a material is strongly dependent on its microstructural characteristics and loading condition. At the atomistic scale, techniques have been developed to study the behavior of a microstructure under shear deformation regarding possible failure modes of the material, such as dislocations,[1] brittle fracture,[2] or shear band formation.[3] The concept of an ideal shear strength in the displacement of adjacent layers of a defect-free crystalline structure was first studied by Frenkel by assuming the energy to shear atoms along a slip plane followed a sinusoidal function.[4] This was later extended to the generalized stacking fault (GSF), which tracks the change in energy as a function of slip plane displacement to shear two rigid blocks of a crystalline structure out of its equilibrium configuration.[5] Rice later identified the unstable stacking fault energy as the maximum energy encountered along the GSF curve, which was utilized to predict ductile-to-brittle transitions.[6] These studies considered the effect of spatial geometry, or crystal structure, on the shear deformation response using simple interaction potentials. Ogata *et al*. compared GSF simulations on two FCC crystals, aluminum and copper, and showed the details of their atomic bonding explained the differences in their ideal strength and deformation behavior under shear.[7] These findings indicate that GSF simulations are capable of probing both the spatial and chemical details of an atomistic model. The method has been widely used to study the shear behavior of a variety of material systems including crystalline,[8] ceramic,[9] and amorphous metallic glass.[10]

In this work, we apply the GSF technique to the atomistic structure of calcium-silicate-hydrates (C-S-H), the main hydration product for Ordinary Portland Cement (OPC) mixtures, which provides the cohesive glue for cementitious materials. The nanoscale details of this material have been widely studied and debated in the literature.[11] Compared to prior studies, the defective nanostructure and ionic-covalent bonding environment within C-S-H contain complexities that have not been investigated through GSF simulations. C-S-H is structurally heterogeneous with both amorphous and crystalline features.[12] Computational studies of C-S-H are largely based on the atomistic model of a defective tobermorite structure developed by Pellenq *et al*., which could explain experimental properties such as nanoindentation stiffness and hardness measurements, solid density, and neutron scattering experiments.[13] This model was updated to include the reactive force field ReaxFF,[14] which was fitted through first principle techniques.[15]

Due to its layered and disordered structure, multiple interfaces exist within C-S-H. This includes interfaces between defective silicate chains, calcium-oxide sheets, and the interlayer region containing water, hydroxyl groups, and calcium ions that separates adjacent silicate layers.[16] This interlayer region, which we refer to as the composite interface due to its inhomogeneous nature, has been studied through molecular dynamic simulations to classify its structural, mechanical, and diffusive properties. The hydrophilic silicate layers result in the composite interface containing highly confined water molecules with an intermediate structure and dynamics similar to a glassy material[17] that is dependent on the chemical composition of the hydrated structure.[18] Prior computational studies have shown that cohesive forces in C-S-H are mostly due to electrostatic

a)Author to whom correspondence should be addressed. Electronic mail: obuyuk@mit.edu

interactions between positively charged calcium ions in the composite interface with the negatively charged silicate layers.[19] These interactions are screened by the presence of water molecules within the composite interface, resulting in localization of strain and a "lubricating effect" under shear deformation.[13] A 3 × 1 × 1 supercell of the Pellenq model using ReaxFF investigated chemical reactions within the C-S-H structure, and found that after water dissociation, the system has a distorted three dimensional glassy structure.[20] The model after dissociation was then studied under large affine shear deformations, which quantified the reduced yield strength and hydrostatic stress behavior compared to its crystalline analog tobermorite.[21] These studies highlight the coupling between spatial structure and chemical bonding that exist within the composite interface of C-S-H.

Motivated by observations that the plastic deformation of C-S-H results in relative sliding of silicate layers,[21] we utilize the GSF approach to take advantage of the heterogeneous quasi-layered nanostructure of C-S-H. This is accomplished by localizing our mechanical perturbation to enforce shear deformation between silicate layers, providing a measure of the traction-displacement relationship along the composite interface. Our implementation is novel in that we consider the slip plane within a disordered multi-atom-layer, whereas prior studies enforce slip to occur across a single-atom-layer of a defect-free crystalline structure. Other researchers have looked at the strength of a sharp interface between a metal and oxide,[22] or the rearrangement of atoms within a purely amorphous metallic glass.[10] This approach allows us to extend the knowledge of both GSF techniques and shear traction-displacement relationships for homogenous crystals to the heterogeneous interfaces of C-S-H. We compare GSF simulations to affine shear loading, where no constraints on the direction of sliding are imposed and strain localization can occur naturally in response to the local compliance and molecular interactions. For both methods, we investigate the system-level response through macroscopic quantities such as stress and displacement, as well as local details such as the rearrangement of atoms throughout the C-S-H structure. The result is a detailed picture of deformation mechanisms within C-S-H and implications on the use of GSF techniques on other material systems with similar spatial and chemical complexity.

II. METHODS

A. GSF formulation

To implement the GSF approach with C-S-H, we follow the formulation of Ogata *et al.*, which was utilized to calculate the ideal shear strength of crystalline Al and Cu through first principles calculations.[7] We separate atoms in our model into two rigid layers based on the locations of the composite interface, and apply a relative slip displacement u between adjacent layers. For each increment of u, we monitor the change in the energy of the system. Our molecular statics calculations are performed at zero temperature, and therefore the total energy of the system is due to the potential energy from atomic interactions. We define the GSF energy $\gamma(u)$, as the change in potential energy $\Delta E(u)$ of the system normalized by the slip plane area A

$$\gamma(u) = \frac{\Delta E(u)}{\mathrm{A}}. \tag{1}$$

For a finite temperature implementation, the Helmholtz free energy replaces the potential energy in Eq. (1). The strain energy density, $\psi(u)$, may be obtained by normalizing the GSF energy by the number of layers, n, being sheared, and the thickness of each layer in the direction perpendicular to the slip plane area h

$$\psi(u) = \frac{\gamma(u)}{nh}. \tag{2}$$

We note that, in Eq. (2), the system volume, $V = nhA$, and that $n = 2$ is associated with a 2 layer model according to the traditional GSF energy definition, and $n \to \infty$ is associated with affine shear deformation of a bulk microstructure.[7,23] From the thermodynamic definition of stress,[24] the average shear stress across the slip plane area can be calculated as the derivative of the strain energy density with respect to applied shear strain $\varepsilon(u) = u/[nh]$. This can be rewritten in terms of the GSF energy defined in Eq. (1) as

$$\tau(\mathrm{u}) = \frac{\partial \psi(u)}{\partial \varepsilon(u)} = \frac{\partial}{\partial u}\gamma(u). \tag{3}$$

The maximum value of τ occurs at the inflection point of the GSF energy defined in Eq. (1), and may be associated with an elastic instability of the structure where the atomic structure is irreversibly changed.[25,26] Past this point, energy is dissipated through inelastic transformational strain.[27] We will use molecular statics simulations to show that for a layered structure, this approach is equivalent to calculating the shear-traction displacement and cohesive interlayer strength at the onset of plastic sliding within the composite interface.

B. Computational methods

Our initial atomic C-S-H configuration was equilibrated for four nanoseconds to allow for water dissociation.[20] We replicate this geometry in the direction perpendicular to the silicate layers (x_3), resulting in a 3 × 1 × 2 supercell of the original Pellenq *et al.* structure. Our model contains 4032 atoms arranged in two disordered layers of silicate chains and calcium oxide sheets separated by the composite interface as shown in Fig. 1. The periodic boundary conditions replicate atoms across the x_3-axis boundary to act as a single layer. The model has a chemical composition of $C_{1.65}SH_{0.77}0.98H_20(C_{1.65}SH_{1.75})$.

All atomistic simulations were performed with the LAMMPS Molecular Dynamics code[28] and the ReaxFF reactive force field[14] utilizing the Reax/C implementation.[29] The ReaxFF interaction parameters for C-S-H have been implemented and validated through prior work on C-S-H and similar material systems.[15,30,31] To equilibrate our structure, we apply an isothermal-isobaric ensemble (NPT) with an external pressure of 0 atm and a temperature of 300 K using a Nose-Hoover thermostat[32] and time step of 0.25 fs with a

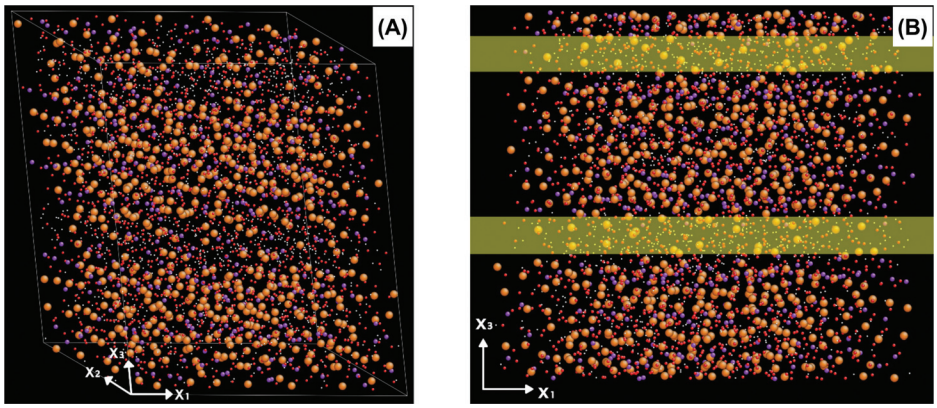

FIG. 1. (a) Three dimensional triclinic simulation cell of the C-S-H model with 4032 atoms represented as colored beads based on atomic weight. Hydrogen is white, oxygen is red, silicon is purple, and calcium is orange. (b) A two-dimensional view of the x_1-x_3 plane allows for visualization of the layered structure. The composite interfaces are identified by the yellow bands.

Verlet integration scheme[33] for 3 ns until the total energy and simulation cell size converged. A 0 atm external pressure was chosen to minimize internal stresses within the structure prior to assessing mechanical properties. Due to the disordered structure of C-S-H, we continue our equilibration for an additional 1 ns to generate a new atomistic structure with statistically identical thermodynamic properties but locally varying atomic positions every 100 ps for a total of 10 unique C-S-H structures. This procedure allows us to assess the sensitivity of our approach. We averaged structural properties of our model over the 1 ns used to generate samples for testing and obtain on average a triclinic box with axes dimensions $39.29 \times 29.40 \times 48.60$ Å, and inclination angles $\alpha = 92.14°$, $\beta = 87.46°$, and $\gamma = 125.39°$. The tetrahedral coordination of silicon atoms within our structure was constant for all C-S-H samples, with normalized Q_n values of $Q_0 = 13\%$, $Q_1 = 62\%$, and $Q_2 = 25\%$, in relative agreement with prior reactive force field models.[20] Reactive force fields have been utilized to observe the dissociation of water molecules throughout the disordered C-S-H structure, and we find that our equilibrated samples had on average 541 ± 5 hydroxyl molecules and 317 ± 2 water molecules.

For each of our 10 initial structures, we compute elastic and inelastic mechanical properties. For elastic constants, we utilize a finite strain approach at zero temperature.[34] Our affine strain deformation ranges from -3% to $+3\%$ with strain increments of 0.5% in the 6 distinct Voigt loading directions. After each strain increment, we relax the system using a steepest descent minimization and evaluate the changes in the virial stress components. We then perform a least square best-fit over the range of applied strain and calculate the components of the stiffness tensor from the derivative of our best fit equation at zero applied strain. We average off-diagonal components which are obtained twice through our calculations. Using this method, we obtain the elastic stiffness tensor (C_{ij}), and its inverse the elastic compliance tensor ($S_{ij} = C_{ij}^{-1}$). This information is used to calculate the Voigt-Reuss-Hill bounds which approximate the effective isotropic elastic properties of the atomistic structure.[35] The Voigt method averages stiffness over all orientations assuming a constant strain which provides an upper bound, whereas the Reuss method averages compliance over all orientations assuming a constant stress and provides a lower bound. The Hill definition is the arithmetic average of the two.

For inelastic behavior, we implement the GSF approach and affine shear as shown in Fig. 2. Both techniques utilize quasi-static loading which is implemented at zero temperature by applying the desired deformation and then relaxing the structure through a steepest descent energy minimization. To implement the GSF formulation described above, we group atoms into layers based on the location of the composite interface, which is defined by examining the locations of silicon atoms along the height of the model (x_3). The atoms contained within these layers were constrained in the direction of applied slip displacement (x_1) but free to move in all other directions, whereas the atoms within the composite interface are fully unconstrained. We apply a relative slip displacement u_1, to the middle layer in steps of 0.01 Å. After each displacement increment, an energy minimization is performed to relax the structure. During relaxation, the atoms contained within the silicate layers are still constrained from

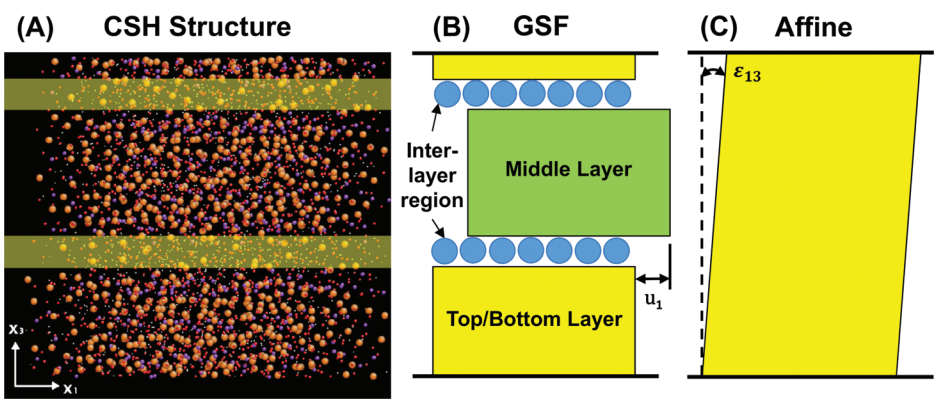

FIG. 2. (a) Schematic showing the two approaches for measuring shear strength of the C-S-H atomistic model. (b) The GSF approach distinguishes the composite interfaces and applies a slip displacement (u_1) to the middle layer, while the top/bottom layer is fixed in the slip direction. (c) The affine shear approach applies slip displacement, which varies linearly along the height of the supercell to be equivalent to an affine shear strain.

TABLE I. Elastic constants of C-S-H samples after equilibration. These elastic constants correspond to the Hill definition of the bulk (K), shear (G), indentation (M), Poisson ratio (ν), and orthotropic Young's moduli. The C-S-H samples are labeled based on total equilibration time in nanoseconds.

C-S-H sample	K (GPa)	G (GPa)	E_1 (GPa)	E_2 (GPa)	E_3 (GPa)	M (GPa)	ν
3.1	48.53	24.56	66.77	75.28	57.22	68.55	0.28
3.2	47.55	25.89	64.18	70.65	62.73	70.89	0.27
3.3	46.79	24.49	64.66	69.21	58.14	67.77	0.28
3.4	47.51	24.85	66.04	70.22	58.45	68.78	0.28
3.5	46.88	24.69	67.52	68.43	57.44	68.21	0.28
3.6	50.98	26.23	72.21	68.28	69.67	72.90	0.28
3.7	47.41	24.10	63.51	70.83	60.21	67.19	0.28
3.8	46.73	24.83	64.64	73.22	58.00	68.43	0.27
3.9	51.60	29.00	71.14	76.75	67.14	78.73	0.26
4.0	50.39	27.23	69.50	75.79	63.87	74.72	0.27
Average	48.44	25.59	67.02	71.87	61.29	70.62	0.28
St. Dev.	1.86	1.54	3.04	3.16	4.40	3.74	0.01
Manzano[20]	48.6	24.7	72.8	74.0	58.3	69.0	0.28

translating in the direction of applied slip displacement. We monitor changes in the potential energy of the system after minimization with respect to the applied displacement according to Eq. (1).

Our second approach applies an affine shear strain to the entire simulation cell through supercell tilting. Deformation was applied in increments of 0.1% strain, and the system was relaxed after each strain increment. After each energy minimization, we compute the stress component in the direction of the applied shear strain. With no kinetic energy, the pressure tensor is associated with the atomic virial stress of the system. This method has been utilized in prior studies of C-S-H under shear.[13,20,21] The affine shear approach applies a linearly varying shear displacement to the entire simulation cell, whereas the GSF approach enforces a uniform displacement across the thickness of the composite interface. To allow for a direct comparison between the two methods, we calculate an equivalent relative displacement across the composite interface for a given applied affine shear strain. Using a simple geometrical relation, the interlayer displacement u_1 is calculated as, $u_1 = \varepsilon_{13} h_{int}$, where ε_{13} is the applied affine shear strain and h_{int} is the thickness of the composite interface.

III. RESULTS

A. Elastic stiffness

From our elastic calculations, we obtain the stiffness and compliance tensors which we use to compute the Voigt-Reuss-Hill bounds. The average and standard deviation for the Hill definition of elastic moduli of our 10 initial C-S-H structures are presented in Table I. Our findings are consistent with other reactive force field studies,[20] validating that our supercell structure of C-S-H containing two silicate layers and composite interfaces is capable of capturing the elastic properties. We compare our computational results with nanoindentation experiments by examining the indentation, or plane stress, modulus and assuming a linear elastic and isotropic material. Our calculated indentation modulus of 70.6 GPa ± 3.7 GPa is within the bounds of experimental values of 65 GPa[36] and 69.0 ± 6.8 GPa[37] for C-S-H with a similar stoichiometry. The reported experimental values have been scaled with linear micromechanics relations to compare with our numerical models of C-S-H.[38,39] Our complete elastic stiffness tensor and additional elastic constants are provided as supplementary material.[40]

B. Inelastic models

After verifying that our C-S-H samples provide consistent elastic properties, we assess the interfacial shear strength along the composite interface. For GSF models, we calculate the GSF energy according to Eq. (1) based on changes in the potential energy of the system. All models show an initial decrease in the total potential energy of the system during the first approximately 0.2 Å of applied slip displacement. A similar behavior has been reported for GSF studies of BCC molybdenum that was attributed to in-plane forces existing along the slip plane,[27,41] which for our C-S-H structure is within the composite interface. The minimum energy observed during this period is utilized as the starting point for subsequent analysis. The resulting GSF energy curves for 5 of our 10 samples are shown in Fig. 3(a).

For each model, a polynomial curve is fit to the GSF energy as a function of slip displacement. When the strain energy changes from concave to convex, the maximum shear strength has been reached and a global elastic instability has occurred to the C-S-H structure, with further external work

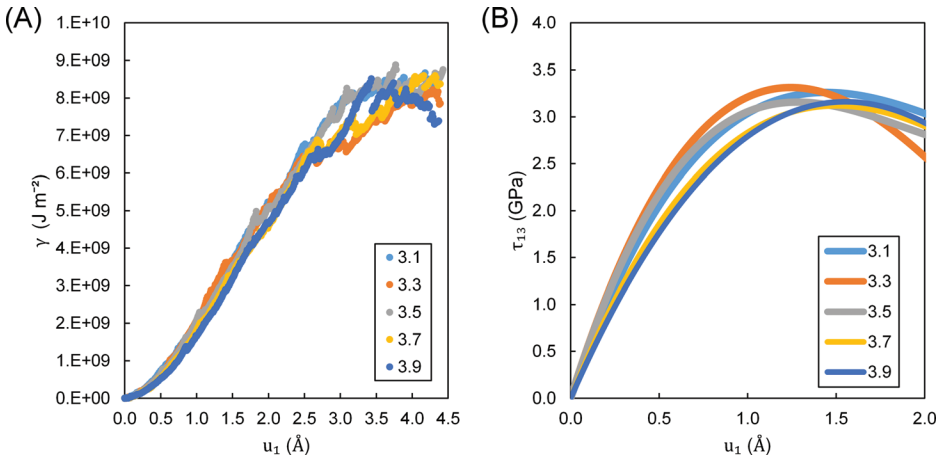

FIG. 3. (a) GSF energy as a function of applied slip displacement. (b) Shear traction-displacement behavior calculated from the derivative of best-fit polynomials to the GSF energy data.

TABLE II. Maximum shear stress and corresponding slip displacement and principal stress components. For each sample, the maximum shear stress (τ_{13}) and corresponding slip displacement (u_1) and change in principal stress components ($\Delta\sigma_1$, $\Delta\sigma_2$, $\Delta\sigma_3$) are shown. The C-S-H samples are labeled based on total equilibration time in nanoseconds.

	GSF					Affine shear				
C-S-H sample	τ_{13} (GPa)	u_1 (Å)	$\Delta\sigma_1$ (GPa)	$\Delta\sigma_2$ (GPa)	$\Delta\sigma_3$ (GPa)	τ_{13} (GPa)	u_1 (Å)	$\Delta\sigma_1$ (GPa)	$\Delta\sigma_2$ (GPa)	$\Delta\sigma_3$ (GPa)
3.1	3.25	1.43	0.00	− 0.06	− 0.19	3.28	1.35	0.33	− 0.14	− 0.58
3.2	3.34	1.43	0.03	− 0.04	− 0.10	3.54	1.09	0.29	− 0.10	− 0.16
3.3	3.31	1.24	0.03	− 0.05	− 0.11	3.46	1.25	0.28	− 0.19	− 0.35
3.4	3.62	1.26	0.00	− 0.05	− 0.14	3.50	0.83	0.33	− 0.02	− 0.05
3.5	3.16	1.28	− 0.01	− 0.08	− 0.17	3.36	1.20	0.28	− 0.19	− 0.30
3.6	3.13	1.53	0.03	− 0.04	− 0.11	3.37	0.87	0.21	− 0.16	− 0.14
3.7	3.12	1.50	− 0.01	− 0.05	− 0.12	3.49	1.60	0.32	− 0.28	− 0.42
3.8	3.40	1.49	0.00	− 0.10	− 0.22	3.68	1.28	0.20	− 0.08	− 0.24
3.9	3.16	1.55	0.03	− 0.03	− 0.21	3.23	1.45	0.31	− 0.11	− 0.32
4.0	3.23	1.37	0.08	− 0.02	− 0.15	3.74	1.39	0.02	− 0.39	− 0.45
Average	3.27	1.41	0.02	− 0.05	− 0.15	3.46	1.23	0.26	− 0.17	− 0.30
St. Dev.	0.15	0.11	0.03	0.03	0.04	0.16	0.24	0.10	0.11	0.16

on the system resulting in plastic energy dissipation through relative sliding of the silicate layers along the composite interface. Other studies on C-S-H structures have indicated that this inelastic strain is facilitated by deformations of water molecules within the composite interface,[42] which we also observe in our own simulations. Prior to the maximum shear strength, local inelastic atomic rearrangements occur, which are observed as small drops in the GSF energy prior to the occurrence of the maximum shear stress. These local rearrangements lead to an increase in the elastic strain energy of the system, which must be due to a reduction in the stress of atoms surrounding the reorganization. A similar observation was made through affine shear simulations on a bulk metallic glass,[43] as well as our own affine shear simulations.

We evaluate the shear stress as a function of slip displacement by calculating the derivative of our fitted GSF energy functions according to Eq. (3). The smooth shear traction-displacement curves obtained for 5 of our 10 samples are shown in Fig. 3(b), and the results of all 10 samples are presented in Table II. We observe a brief initial linear behavior followed by nonlinear strain hardening until the maximum shear stress along the interface is reached. We obtain an average maximum shear stress of 3.27 GPa ± 0.15 GPa at an applied slip displacement of 1.41 Å ± 0.11 Å. Following the maximum shear stress, a strain softening behavior is observed, which decreases and then fluctuates around zero stress for slip displacements greater than approximately 3.0 to 3.5 Å. For these large slip displacements, the GSF energy has plateaued, signifying that the elastic strain energy of the system is saturated and further external work is dissipated through inelastic sliding. The shear stress calculated according to Eq. (3) is only applicable to changes in stored elastic strain energy of Eq. (1), and is therefore unable to account for the shear traction in the interlayer region due to dissipated energy from plastic deformations.

For the affine shear models, we compute the component of the virial stress corresponding to our applied shear strain and plot it as a function of the equivalent relative interlayer slip displacement as shown in Fig. 4. The stress-displacement curve shows many of the same features as those obtained with the GSF approach. We observe an initial linear slope extending to approximately 0.25 Å of slip, followed by nonlinear strain hardening up to the maximum shear strength with multiple stress drops occurring along the curve. These stress drops coincide with drops in GSF energy previously observed due to local inelastic rearrangements that enhanced the elastic strain energy of the material, and would be observed as a reduction in the atomistic stress. A physical interpretation of this avalanche-type behavior is that the accumulation of stress within the structure leads to transitions between metastable states.[44]

The identification of a maximum shear stress is less straightforward for affine shear models due to the increasing

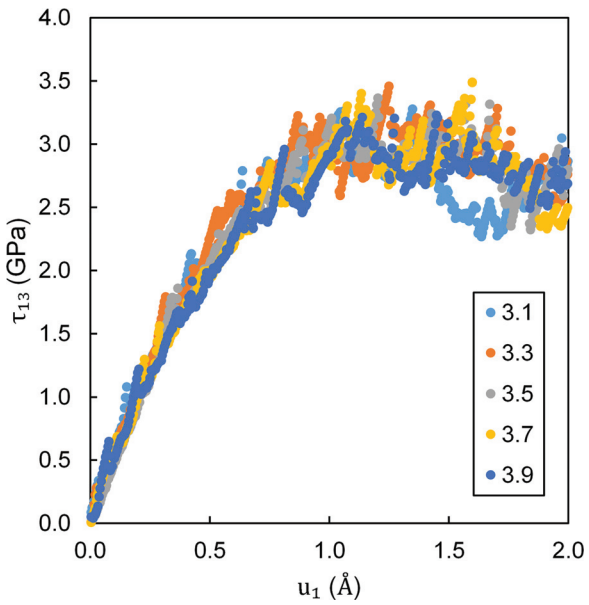

FIG. 4. Shear stress-displacement behavior for affine shear models.

frequency and magnitude of stress drops as the stress-displacement curve reaches a relatively perfectly plastic plateau. This regime was observed in prior studies and has been attributed to a stick-slip behavior during the relative plastic sliding of silicate layers "lubricated" by the confined water and hydroxyl molecules in the composite interface.[20,21] To compare with GSF models, we identify the peak stress observed during each simulation. However, we note that many samples show multiple stress peaks of very similar magnitude at slightly different applied slip displacements. We find an average maximum shear strength of 3.46 GPa $\pm$ 0.16 GPa and corresponding relative slip displacement of 1.23 Å $\pm$ 0.24 Å. Results from all C-S-H samples are presented in Table II.

We observe excellent agreement between the maximum shear strength and corresponding slip displacement computed with the GSF and affine shear approach. Our results are also consistent with those obtained through affine shear loading of a $3 \times 1 \times 1$ supercell of the Pellenq model and a reactive force field.[20,21] Similar to these prior reactive studies, we also observe some reorganization of water and hydroxyl groups within the composite interface under large shear deformations for both GSF and affine models. However, the change in the number of molecules is typically less than 1%, and therefore likely has a small effect on the overall system behavior. On average, affine shear models predict a maximum shear stress that is a 5.8% larger than GSF models. However, we also observe that the principal stress components deviate more for affine shear loading than for GSF, which would lead to an increase in the predicted maximum shear strength for a cohesive-frictional material due to changes in confining pressure. This observation is investigated in detail in Section III C.

C. Principal stress behavior

Fig. 5 shows the differences in the behavior of virial principal stress components along with the computed shear stress during loading of a representative sample. The direction of stress components are defined with respect to the coordinate system (x_1, x_2, x_3) and corresponding atomic displacements (u_1, u_2, u_3) shown in Fig. 1. Because these stresses are initially non-zero and vary slightly between C-S-H samples, we plot the relative change with respect to their initial magnitude, e.g., $\Delta\sigma_i = \sigma_i(u) - \sigma_i(u = 0)$, where $\sigma_i(u)$ is principal stress component i at slip displacement u, and $u = 0$ is the initial undeformed configuration.

The stresses in the direction parallel to the applied slip displacement (σ_1) show both quantitative and qualitative differences between our two methods of loading. Our GSF implementation constrains atoms in the slip direction by setting the corresponding force component to zero, allowing us to rigidly displace the blocks of atoms. This methodology limits the virial stress component reported for the GSF approach to only contain contributions from atoms within the composite interface, while the affine shear method includes forces computed from all atoms within the supercell. Therefore, the limited change in σ_1 exhibited by GSF results is indicative of the compliance of the interface. Affine shear simulations show an increasing trend of σ_1 with increasing shear deformation until the maximum shear stress is reached, after which a generally decreasing trend is observed for further slip displacement. This suggests that the build-up of σ_1 observed for affine shear models is due to strain within the silicate layers, which is prevented with our GSF approach, and that much of this strain is elastically released along with the onset of inelastic sliding, when the cohesive shear strength of the composite interface is overcome.

For both GSF and affine shear models, the principal stress components normal to the direction of applied slip displacement (σ_2, σ_3) initially show relatively little change or slight dilation, followed by a negative trend as the shear stress response becomes increasingly nonlinear. The decrease in principal stresses has been previously observed in C-S-H, and indicates that the structure tends towards compaction under large shear deformation.[21] The stress perpendicular to the plane of the C-S-H layers (σ_3) shows the highest sensitivity to shear deformation. The σ_3 stress is normal to the failure plane defined by the composite interface, suggesting that a Mohr-Coulomb failure criterion may be appropriate at the atomistic scale as has been previously applied to C-S-H models utilizing the empirical force field CSH-FF.[37] However, the variation in other principal stress terms may indicate that a modified Mohr-Coulomb model is also suitable, as has been suggested for amorphous metallic

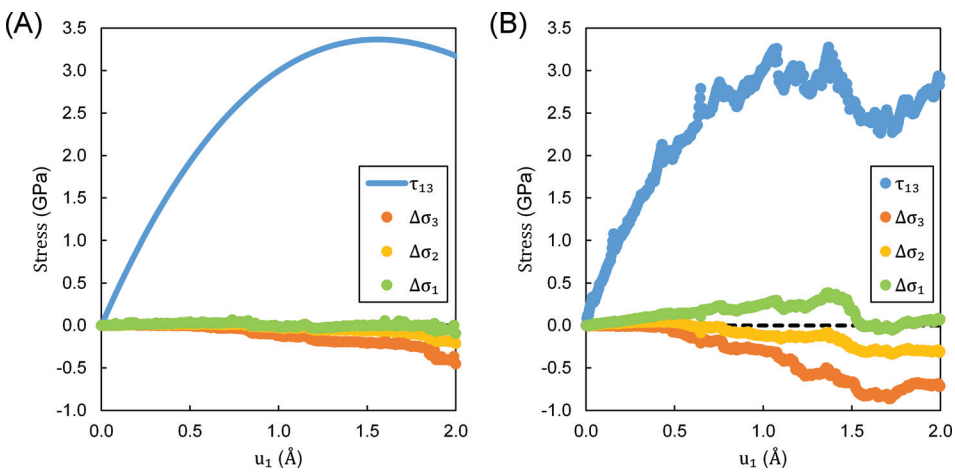

FIG. 5. Comparison of shear stress and relative change in principal stress components with respect to applied shear deformation for (a) GSF loading and (b) affine shear loading.

glasses.[43,45] Mohr-Coulomb type models are commonly used to describe the strength asymmetry in yield and failure of cementitious materials at the macroscale.

Fig. 6 shows a comparison of the changes in principal stress components for 5 of the C-S-H samples under GSF and affine shear. For all principal stress components, affine shear models exhibit a greater sensitivity to shear deformation than GSF models, which we attribute to the fluctuating nature of the stress-displacement response for affine shear. Although the stress-displacement response for GSF models is perfectly smooth due to our polynomial curve-fitting procedure, the GSF energy curves (Fig. 3(a)) of the raw data are relatively smooth up to approximately 2 Å of slip displacement. This indicates that a greater number of atomic rearrangements are occurring for affine shear loading, and explains the increasing trends towards compaction of the overall structure as atoms transition between metastable configurations. We also note that there is a greater variance in principal stress components between different C-S-H samples for affine shear compared to GSF, demonstrating that the approach is more sensitive to differences in the initial internal structure.

To further investigate these results, we monitor the displacement of individual atoms within the C-S-H structure. Figs. 7 and 8 show the computed displacements for each atom type from a representative C-S-H structure at the maximum shear stress for both GSF and affine shear loading. Displacements perpendicular to the layered C-S-H structure (u_3), and out-of-plane with respect to the applied slip displacement (u_2), are plotted with respect to the position of the atoms along the height of the simulation cell (x_3). The boundaries of the composite interface are shown as shaded bands at their appropriate elevations. The greatest atomic displacements are observed within the composite interface for both approaches. As expected from the principal stress behavior, the magnitude of displacements is much greater for affine shear loading when compared to GSF, for both the composite interface and throughout the C-S-H structure.

We can investigate the deformation behavior at multiple interfaces within C-S-H by examining the displacements of specific atom types. Hydrogen and oxygen atoms show the largest displacements in both the composite interface as well as within the layers containing silicate chains. The atoms of the latter case are associated with intralayer water within a

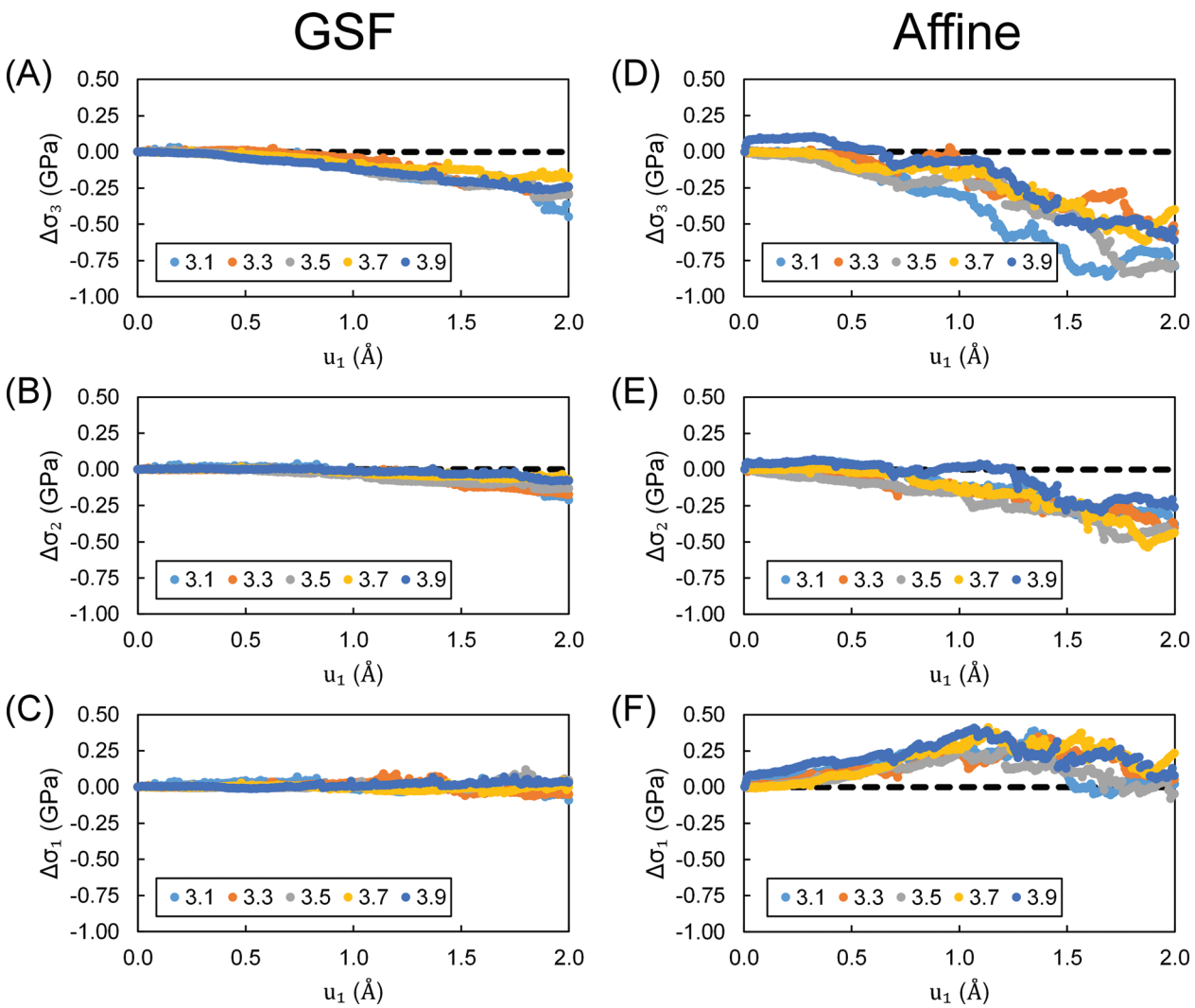

FIG. 6. Relative changes in principal stress components for five C-S-H samples under GSF and affine shear loading. $\Delta\sigma_1$ is in the direction of applied displacement, $\Delta\sigma_2$ is out-of-plane with respect to shear deformation, and $\Delta\sigma_3$ is normal to the plane of the composite interface.

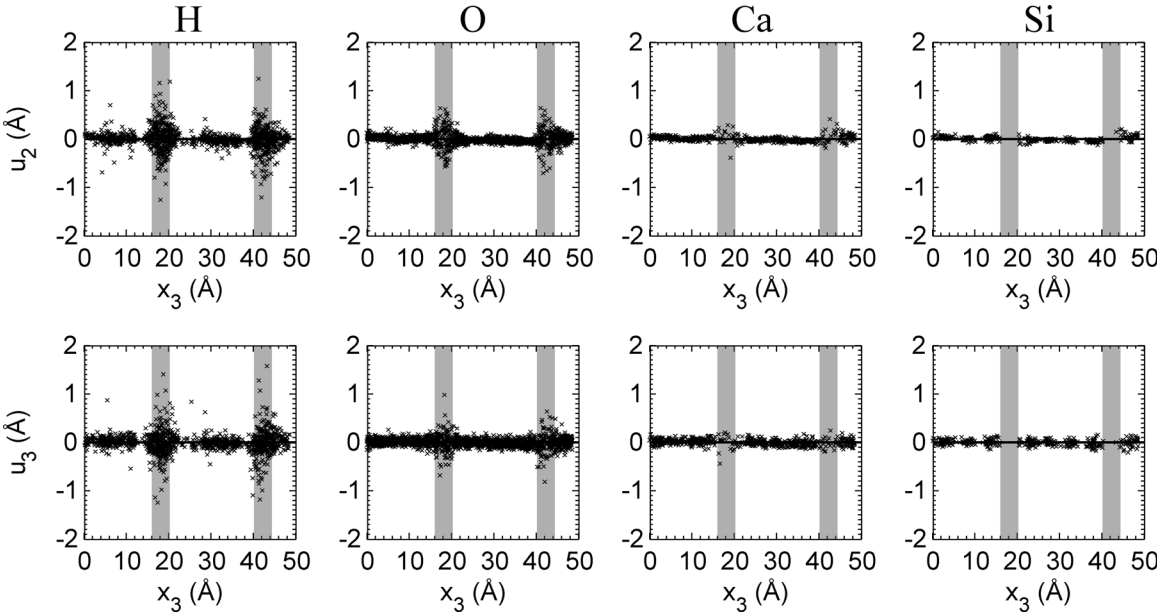

FIG. 7. Displacement of individual atoms at the maximum shear stress for a single C-S-H structure under GSF loading. Atoms shown are hydrogen (H), oxygen (O), calcium (Ca), and silicon (Si). The shaded areas indicate the interlayer region. The displacement u_2 is out-of-plane with respect to shear deformation, and u_3 is normal to the plane of the composite interface.

region that has been referred to as the disconnected small pore space.[20] These atoms are weakly bonded to the surrounding structure and therefore exhibit the greatest deformation and extent of rearrangement. Calcium and silicon atoms which form the partially crystalline layers show the least displacement under shear loading. This is especially true for the GSF approach indicating that very little compaction behavior is occurring within the partially crystalline features, and the compaction that was observed is largely due to atomic rearrangements in the composite interface. These local observations agree with macroscale principal stress behavior, and support that GSF load results in a reduced coupling between shear and principal stress behavior.

If we assume that atomistic C-S-H follows a Mohr-Coulomb model for a cohesive-frictional material, we may use our results to calculate the internal friction coefficient describing the normal-stress dependency of the shear stress, as well as the cohesion describing the shear stress for zero confining pressure. Fig. 9 shows the maximum shear stress (τ_{13}) and corresponding normal confining stress (σ_3) for both affine shear and GSF models. A negative σ_3 is indicative of a compressive pressure being applied to the slip plane, while a

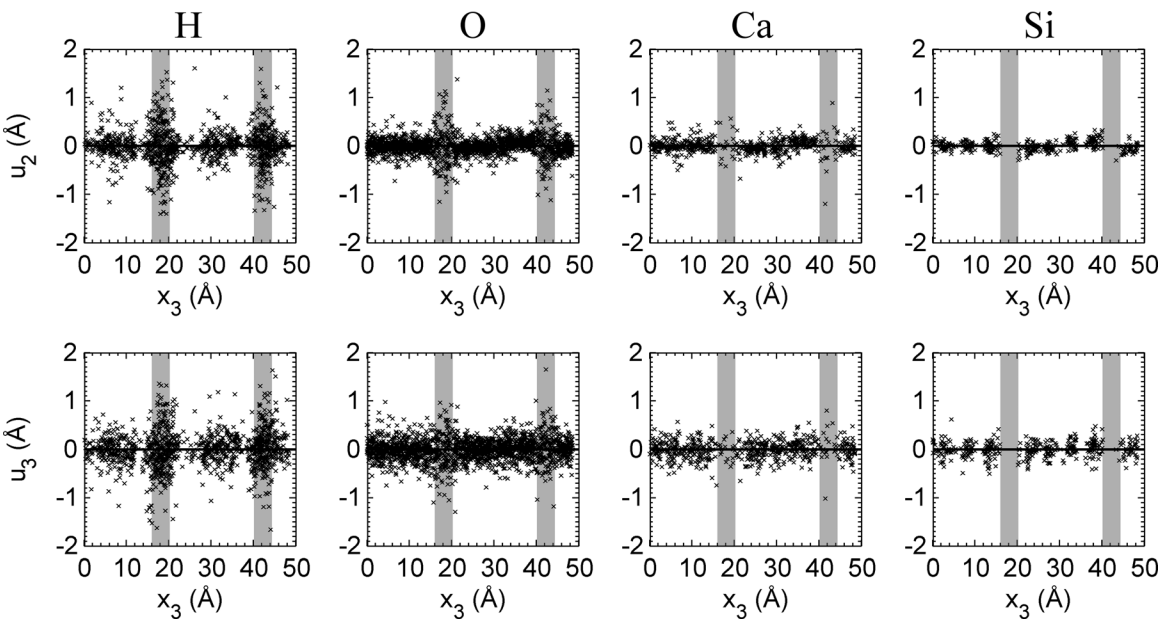

FIG. 8. Displacement of individual atoms at the maximum shear stress for a single C-S-H structure under affine shear loading. The same conventions shown in Fig. 7 are utilized.

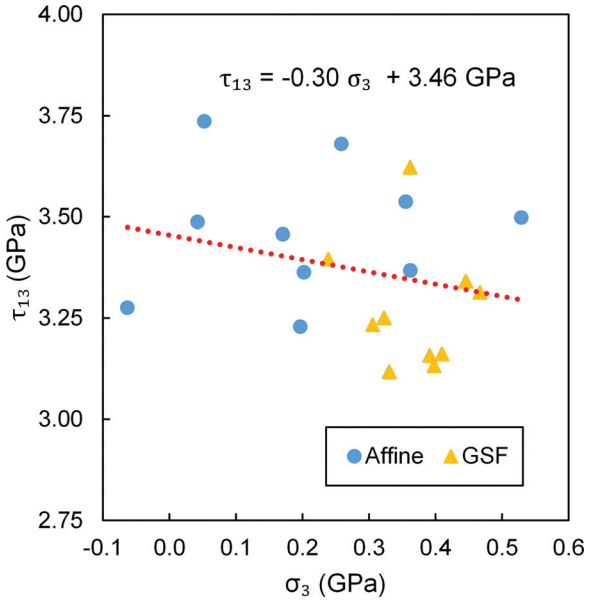

FIG. 9. A Mohr-Coulomb model fit to affine shear and GSF maximum shear stress (τ_{13}) results for all of our C-S-H samples.

positive value is associated with a tensile disjoining pressure. The affine shear results span a larger range of confining pressures due to the greater changes in normal stress behavior under shear loading, as well as the larger variance in slip displacement at the observed maximum shear stress. We apply a linear best-fit equation to all of our data points and obtain a Mohr-Coulomb relationship with an internal friction coefficient of 0.30 and cohesion of 3.46 GPa. These results demonstrate that the differences in the averaged maximum shear stress between the affine shear and GSF approach may be explained by the normal stress dependency of the material.

IV. DISCUSSION

Despite the differences in methodology between affine shear and GSF loading, we find many similarities in the stress-displacement response. Our results suggest that the inelastic strength and deformation properties of the bulk C-S-H structure are governed by the behavior along the composite interface. The composite interface between layers of silicate chains may be considered as a defect within the C-S-H structure. Whereas affine shear loading considers C-S-H as a homogenous structure, our GSF approach takes advantage of the layered texture of C-S-H to isolate the mechanical response at this location.

As part of this study, we investigated the connection between local atomic deformations with the global stress-displacement response of the C-S-H structure to explain variations in the compaction behavior under shear deformation. These details support the reduced coupling between shear and principal stress component deformation observed for GSF loading, as well as the repeated and collective rearrangement of atoms to metastable configurations observed for affine shear. Furthermore, this methodology allowed us to assess the influence of multiple interfaces, both crystalline and amorphous, within the C-S-H structure by modifying our applied perturbation. The ability to understand and connect fundamental microstructural behavior with its global structural response is an application of mesoscale science.[46] This approach is essential to developing multiscale models of complex hierarchical materials.

The traction-displacement response of materials may be utilized to define interactions at larger length scales. For this purpose, we have shown that the GSF technique is appealing for heterogeneous materials due to its ability to assess the mechanical behavior and limiting strength at selected interfaces within an atomistic structure. Previous studies of C-S-H have used interactions observed through affine shear simulations in a multi-scale framework to develop a coarse-grained interaction potential to describe elastic properties on the scale of hundreds of nanometers.[47] However, for cement paste systems, the inelastic behavior of C-S-H at larger length scales have only been accurately described through nonlinear micromechanics models and nonreactive force fields.[37] Nonlinear micromechanics models make assumptions regarding the microstructure characteristics of C-S-H on the order of hundreds of nanometers, so the development of a computational model at this scale that could capture both elastic and inelastic behaviors of the material would strengthen these models and allow for a greater understanding of the role of gel and capillary porosity on the deformation behavior of C-S-H. This challenge may be met with a coarse-grained model incorporating atomic interactions probed from reactive force field models.

To utilize the GSF approach for multiscale modelling of C-S-H, further research is required to assess discrepancies between the atomistic results and experiments. Despite agreement with elastic properties computed for the atomistic C-S-H structure with nanoindentation stiffness measurements, our Mohr-Coulomb model describing inelastic behavior indicates that the calculated cohesion strength of 3.46 GPa is much greater than values ranging from 0.34 to 0.50 GPa predicted from nanoindentation hardness measurements and scaling relations.[39] For defect-free crystalline systems, the shear strength calculated through first principles or molecular dynamic simulations at zero temperature is often referred to as the ideal strength. Therefore, the strength measured here may be considered as an ideal strength obtained for the atomistic C-S-H structure. The ideal strength shows some dependency on the specific configurations of the defects existing along the composite interface as observed through the variation in calculated mechanical properties between samples. We do observe that our calculated normal-stress dependency of 0.30 is close to the upper bound of experimental values ranging from of 0.18 to 0.28 that were scaled from nanoindentation tests.[39] In future work, we will further study the behavior of C-S-H under a wider range of multiaxial loading conditions to further assess the applicability of a Mohr-Coulomb law, and perform finite temperature simulations to assess the effect on the traction-displacement response.

Motivated by our success with implementing the GSF technique for C-S-H, we believe that this approach may also be applied to other material systems containing heterogeneous structures or composite interfaces. Similar systems include graphene and polymer structures, collagen and

hydroxyapatite in bone, and biological materials with organic and inorganic interfaces. The cohesive strength of these interfaces at the atomistic scale control many of the deformation and fracture properties that are observed at the macroscale, and this technique could be a valuable tool for further studies and applications.

V. CONCLUSIONS

To study inelastic shear behavior, we implemented the GSF technique for a heterogeneous material by enforcing a failure plane along a composite interface within the quasi-layered structure of C-S-H. These simulations were compared to affine shear deformations, which treated C-S-H as a homogenous structure and applied no additional constraints. Through our investigation, we find the following:

(1) A GSF methodology can be used to isolate strain along a composite interface within a heterogeneous structure, such as the interlayer region separating silicate layers in C-S-H, in order to calculate the shear traction as a function of applied displacement or strain.
(2) GSF techniques which have been developed for relatively simple, defect-free and homogenous crystals may be readily applied to a disordered heterogeneous material with the spatial and chemical complexity of C-S-H.
(3) For atomistic models of C-S-H, GSF loading is able to clearly predict the maximum strength at the onset of plastic sliding between layers in close agreement with affine shear calculations. This suggests that the interfacial strength within the composite interface controls bulk shear strength properties of the Pellenq *et al*. atomistic C-S-H model.
(4) For GSF loading, the limitation of strain away from the composite interface results in a reduced coupling between shear and compaction behavior of the C-S-H structure when compared to affine shear simulations. This leads to less fluctuations in the strain energy and stress of the system from local rearrangements of atoms within the partially crystalline silicate layers and calcium oxide sheets.
(5) Variation in principal stress components under shear deformation is indicative of a Mohr-Coulomb type failure model, and the behavior is dependent on the selected shear loading methodology.

ACKNOWLEDGMENTS

We acknowledge the "Kuwait Foundation for the Advancement of Sciences" and "Kuwait-MIT Center for Natural Resources and the Environment" for support during this work. In addition, S.D.P. acknowledges helpful discussions with Dr. E. Masoero.

[1]H. Van Swygenhoven, P. Derlet, and A. Frøseth, Nat. Mater. **3**, 399 (2004).
[2]M. J. Buehler, F. F. Abraham, and H. Gao, Nature **426**, 141 (2003).
[3]A. Greer, Y. Cheng, and E. Ma, Mater. Sci. Eng., R **74**, 71 (2013).
[4]J. Frenkel, Z. Phys. **37**, 572 (1926).
[5]V. Vitek, Philos. Mag. **18**, 773 (1968).
[6]J. R. Rice, J. Mech. Phys. Solids **40**, 239 (1992).
[7]S. Ogata, J. Li, and S. Yip, Science **298**, 807 (2002).
[8]J. A. Zimmerman, H. Gao, and F. F. Abraham, Modell. Simul. Mater. Sci. Eng. **8**, 103 (2000).
[9]P. Hirel, P. Marton, M. Mrovec, and C. Elsässer, Acta Mater. **58**, 6072 (2010).
[10]F. Shimizu, S. Ogata, and J. Li, Acta Mater. **54**, 4293 (2006).
[11]S. Papatzani, K. Paine, and J. Calabria-Holley, Constr. Build. Mater. **74**, 219 (2015).
[12]M. Bauchy, M. J. Qomi, F. J. Ulm, and R. J. Pellenq, J. Chem. Phys. **140**, 214503 (2014).
[13]R. J. Pellenq, A. Kushima, R. Shahsavari, K. J. Van Vliet, M. J. Buehler, S. Yip, and F. J. Ulm, Proc. Natl. Acad. Sci. U.S.A. **106**, 16102 (2009).
[14]A. C. Van Duin, S. Dasgupta, F. Lorant, and W. A. Goddard, J. Phys. Chem. A **105**, 9396 (2001).
[15]H. Manzano, R. J. Pellenq, F. J. Ulm, M. J. Buehler, and A. C. van Duin, Langmuir **28**, 4187 (2012).
[16]H. M. Jennings, J. J. Thomas, J. S. Gevrenov, G. Constantinides, and F.-J. Ulm, Cem. Concr. Res. **37**, 329 (2007).
[17]M. Youssef, R. J. Pellenq, and B. Yildiz, J. Am. Chem. Soc. **133**, 2499 (2011).
[18]M. J. Qomi, M. Bauchy, F. J. Ulm, and R. J. Pellenq, J. Chem. Phys. **140**, 054515 (2014).
[19]R.-M. Pellenq, N. Lequeux, and H. Van Damme, Cem. Concr. Res. **38**, 159 (2008).
[20]H. Manzano, S. Moeini, F. Marinelli, A. C. van Duin, F. J. Ulm, and R. J. Pellenq, J. Am. Chem. Soc. **134**, 2208 (2012).
[21]H. Manzano, E. Masoero, I. Lopez-Arbeloa, and H. M. Jennings, Soft Matter **9**, 7333 (2013).
[22]Y. Jiang, Y. Wei, J. R. Smith, J. W. Hutchinson, and A. G. Evans, Int. J. Mater. Res. **101**, 8 (2010).
[23]J. Li, A. H. Ngan, and P. Gumbsch, Acta Mater. **51**, 5711 (2003).
[24]M. J. Buehler, *Atomistic Modeling of Materials Failure* (Springer, 2008).
[25]J. Wang, J. Li, S. Yip, S. Phillpot, and D. Wolf, Phys. Rev. B **52**, 12627 (1995).
[26]J. Li, K. J. Van Vliet, T. Zhu, S. Yip, and S. Suresh, Nature **418**, 307 (2002).
[27]S. Ogata, J. Li, and S. Yip, Phys. Rev. B **71**, 224102 (2005).
[28]S. Plimpton, J. Comput. Phys. **117**, 1 (1995).
[29]H. M. Aktulga, J. C. Fogarty, S. A. Pandit, and A. Y. Grama, Parallel Comput. **38**, 245 (2012).
[30]J. C. Fogarty, H. M. Aktulga, A. Y. Grama, A. C. Van Duin, and S. A. Pandit, J. Chem. Phys. **132**, 174704 (2010).
[31]M. C. Pitman and A. C. Van Duin, J. Am. Chem. Soc. **134**, 3042 (2012).
[32]S. Nosé and M. Klein, Mol. Phys. **50**, 1055 (1983).
[33]L. Verlet, Phys. Rev. **159**, 98 (1967).
[34]O. H. Nielsen and R. M. Martin, Phys. Rev. Lett. **50**, 697 (1983).
[35]R. Hill, Proc. Phys. Soc. London, Sect. A **65**, 349 (1952).
[36]M. J. DeJong and F.-J. Ulm, Cem. Concr. Res. **37**, 1 (2007).
[37]M. J. Abdolhosseini Qomi, K. J. Krakowiak, M. Bauchy, K. L. Stewart, R. Shahsavari, D. Jagannathan, D. B. Brommer, A. Baronnet, M. J. Buehler, S. Yip, F. J. Ulm, K. J. Van Vliet, and R. J. Pellenq, Nat. Commun. **5**, 4960 (2014).
[38]G. Constantinides and F.-J. Ulm, J. Mech. Phys. Solids **55**, 64 (2007).
[39]F. J. Ulm, M. Vandamme, C. Bobko, J. A. Ortega, K. Tai, and C. Ortiz, J. Am. Ceram. Soc. **90**, 2677 (2007).
[40]See supplementary material at http://dx.doi.org/10.1063/1.4926870 for detailed results of our elastic calculations.
[41]M. Mrovec, T. Ochs, C. Elsässer, V. Vitek, D. Nguyen-Manh, and D. G. Pettifor, Z. Metallkd. **94**, 244 (2003).
[42]M. J. Abdolhosseini Qomi, F. J. Ulm, and R. J. M. Pellenq, J. Am. Ceram. Soc. **95**, 1128 (2012).
[43]S. Ogata, F. Shimizu, J. Li, M. Wakeda, and Y. Shibutani, Intermetallics **14**, 1033 (2006).
[44]P. Bak and K. Chen, Sci. Am. **264**, 46 (1991).
[45]H. Ruan, L. Zhang, and J. Lu, Int. J. Solids Struct. **48**, 3112 (2011).
[46]S. Yip and M. P. Short, Nat. Mater. **12**, 774 (2013).
[47]E. Masoero, E. Del Gado, R. J. M. Pellenq, F. J. Ulm, and S. Yip, Phys. Rev. Lett. **109**, 155503 (2012).